
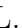













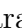

















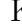
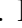
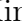

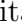


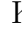























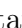





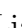




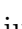















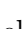
























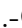












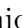







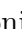





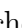





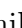

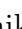



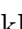
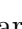











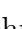





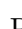
































Measurement of the Branching Fraction of $\Lambda_c^+ \rightarrow pK_S^0\pi^0$ at Belle

I. Adachi , L. Aggarwal , H. Ahmed , J. K. Ahn , H. Aihara , N. Akopov ,
M. Alhakami , A. Aloisio , N. Althubiti , M. Angelsmark , N. Anh Ky ,
D. M. Asner , H. Atmacan , T. Aushev , V. Aushev , M. Aversano , R. Ayad ,
V. Babu , H. Bae , N. K. Baghel , S. Bahinipati , P. Bambade , Sw. Banerjee ,
M. Barrett , M. Bartl , J. Baudot , A. Baur , A. Beaubien , F. Becherer ,
J. Becker , J. V. Bennett , F. U. Bernlochner , V. Bertacchi , M. Bertemes ,
E. Bertholet , M. Bessner , S. Bettarini , V. Bhardwaj , B. Bhuyan , F. Bianchi ,
T. Bilka , D. Biswas , A. Bobrov , D. Bodrov , A. Bolz , A. Bondar , J. Borah ,
A. Boschetti , A. Bozek , M. Bračko , P. Branchini , R. A. Briere , T. E. Browder ,
A. Budano , S. Bussino , Q. Campagna , M. Campajola , L. Cao , G. Casarosa ,
C. Cecchi , J. Cerasoli , M.-C. Chang , P. Chang , P. Cheema , B. G. Cheon ,
K. Chilikin , K. Chirapatpimol , H.-E. Cho , K. Cho , S.-J. Cho , S.-K. Choi ,
S. Choudhury , J. Cochran , L. Corona , J. X. Cui , E. De La Cruz-Burelo ,
S. A. De La Motte , G. De Nardo , G. De Pietro , R. de Sangro , M. Destefanis ,
S. Dey , R. Dhamija , A. Di Canto , F. Di Capua , J. Dingfelder , Z. Doležal ,
I. Domínguez Jiménez , T. V. Dong , D. Dossett , S. Dubey , K. Dugic ,
G. Dujany , P. Ecker , D. Epifanov , J. Eppelt , P. Feichtinger , T. Ferber ,
T. Fillinger , C. Finck , G. Finocchiaro , F. Forti , A. Frey , B. G. Fulsom ,
A. Gabrielli , E. Ganiev , M. Garcia-Hernandez , G. Gaudino , V. Gaur , A. Gaz ,
A. Gellrich , G. Ghevondyan , D. Ghosh , H. Ghumaryan , G. Giakoustidis ,
R. Giordano , A. Giri , P. Gironella Gironell , A. Glazov , B. Gobbo , R. Godang ,
O. Gogota , P. Goldenzweig , E. Graziani , D. Greenwald , Z. Gruberová ,
Y. Guan , K. Gudkova , I. Haide , S. Halder , Y. Han , C. Harris , K. Hayasaka ,
H. Hayashii , S. Hazra , M. T. Hedges , A. Heidelberg , I. Heredia de la Cruz ,
M. Hernández Villanueva , T. Higuchi , M. Hoek , M. Hohmann , R. Hoppe ,
P. Horak , C.-L. Hsu , T. Humair , T. Iijima , K. Inami , N. Ipsita , A. Ishikawa ,
R. Itoh , M. Iwasaki , P. Jackson , D. Jacobi , W. W. Jacobs , E.-J. Jang , S. Jia ,
Y. Jin , A. Johnson , K. K. Joo , H. Junkerkalefeld , M. Kaleta , J. Kandra ,
K. H. Kang , G. Karyan , T. Kawasaki , F. Keil , C. Ketter , C. Kiesling

C.-H. Kim , D. Y. Kim , J.-Y. Kim , K.-H. Kim , Y.-K. Kim , Y. J. Kim ,
 H. Kindo , K. Kinoshita , P. Kodyš , T. Koga , S. Kohani , K. Kojima ,
 A. Korobov , S. Korpar , E. Kovalenko , P. Križan , P. Krokovny , T. Kuhr ,
 Y. Kulii , D. Kumar , M. Kumar , R. Kumar , K. Kumara , T. Kunigo ,
 A. Kuzmin , Y.-J. Kwon , S. Lacaprara , Y.-T. Lai , K. Lalwani , T. Lam ,
 J. S. Lange , T. S. Lau , M. Laurenza , R. Lebourcher , F. R. Le Diberder ,
 M. J. Lee , C. Lemettai , P. Leo , C. Li , L. K. Li , Q. M. Li , W. Z. Li , Y. Li ,
 Y. B. Li , Y. P. Liao , J. Libby , J. Lin , S. Lin , M. H. Liu , Q. Y. Liu ,
 Y. Liu , Z. Q. Liu , D. Liventsev , S. Longo , C. Lyu , Y. Ma , C. Madaan ,
 M. Maggiora , S. P. Maharana , R. Maiti , G. Mancinelli , R. Manfredi ,
 E. Manoni , M. Mantovano , D. Marcantonio , S. Marcello , C. Marinas ,
 C. Martellini , A. Martens , A. Martini , T. Martinov , L. Massaccesi ,
 M. Masuda , D. Matvienko , S. K. Maurya , M. Maushart , J. A. McKenna ,
 R. Mehta , F. Meier , D. Meleshko , M. Merola , C. Miller , M. Mirra , S. Mitra ,
 K. Miyabayashi , H. Miyake , R. Mizuk , G. B. Mohanty , S. Mondal ,
 S. Moneta , H.-G. Moser , R. Mussa , I. Nakamura , M. Nakao , H. Nakazawa ,
 Y. Nakazawa , M. Naruki , Z. Natkaniec , A. Natochii , M. Nayak , G. Nazaryan ,
 M. Neu , S. Nishida , S. Ogawa , H. Ono , Y. Onuki , F. Otani , P. Pakhlov ,
 G. Pakhlova , E. Paoloni , S. Pardi , K. Parham , H. Park , J. Park , K. Park ,
 S.-H. Park , B. Paschen , A. Passeri , S. Patra , T. K. Pedlar , I. Peruzzi ,
 R. Peschke , R. Pestotnik , M. Piccolo , L. E. Piilonen , P. L. M. Podesta-Lerma ,
 T. Podobnik , S. Pokharel , C. Praz , S. Prell , E. Prencipe , M. T. Prim ,
 I. Prudiiev , H. Purwar , P. Rados , G. Raeuber , S. Raiz , N. Rauls ,
 K. Ravindran , J. U. Rehman , M. Reif , S. Reiter , M. Remnev , L. Reuter ,
 D. Ricalde Herrmann , I. Ripp-Baudot , G. Rizzo , M. Roehrken , J. M. Roney ,
 A. Rostomyan , N. Rout , D. A. Sanders , S. Sandilya , L. Santelj , Y. Sato ,
 V. Savinov , B. Scavino , J. Schmitz , S. Schneider , G. Schnell , M. Schnepf ,
 K. Schoenning , C. Schwanda , A. J. Schwartz , Y. Seino , A. Selce , K. Senyo ,
 J. Serrano , M. E. Sevier , C. Sfienti , W. Shan , C. Sharma , X. D. Shi ,
 T. Shillington , T. Shimasaki , J.-G. Shiu , D. Shtol , A. Sibidanov , F. Simon 

J. B. Singh , J. Skorupa , M. Sobotzik , A. Soffer , A. Sokolov , E. Solovieva ,
 S. Spataro , B. Spruck , W. Song , M. Starič , P. Stavroulakis , S. Stefkova ,
 R. Stroili , J. Strube , Y. Sue , M. Sumihama , K. Sumisawa , W. Sutcliffe ,
 N. Suwonjandee , H. Svidras , M. Takahashi , M. Takizawa , U. Tamponi ,
 K. Tanida , F. Tenchini , A. Thaller , O. Tittel , R. Tiwary , E. Torassa ,
 K. Trabelsi , I. Tsaklidis , M. Uchida , I. Ueda , T. Uglov , K. Unger , Y. Unno ,
 K. Uno , S. Uno , P. Urquijo , Y. Ushiroda , S. E. Vahsen , R. van Tonder ,
 M. Veronesi , A. Vinokurova , V. S. Vismaya , L. Vitale , V. Vobbiliseti ,
 R. Volpe , A. Vossen , M. Wakai , S. Wallner , M.-Z. Wang , X. L. Wang ,
 Z. Wang , A. Warburton , M. Watanabe , S. Watanuki , C. Wessel , E. Won ,
 X. P. Xu , B. D. Yabsley , S. Yamada , W. Yan , S. B. Yang , J. Yelton ,
 J. H. Yin , K. Yoshihara , C. Z. Yuan , J. Yuan , L. Zani , F. Zeng , B. Zhang ,
 V. Zhilich , J. S. Zhou , Q. D. Zhou , L. Zhu , V. I. Zhukova , and R. Žlebčik 

(The Belle and Belle II Collaborations)

We report a precise measurement of the ratio of branching fractions $\mathcal{B}(\Lambda_c^+ \rightarrow pK_S^0\pi^0)/\mathcal{B}(\Lambda_c^+ \rightarrow pK^-\pi^+)$ using 980 fb⁻¹ of e^+e^- data from the Belle experiment. We obtain a value of $\mathcal{B}(\Lambda_c^+ \rightarrow pK_S^0\pi^0)/\mathcal{B}(\Lambda_c^+ \rightarrow pK^-\pi^+) = 0.339 \pm 0.002 \pm 0.009$, where the first and second uncertainties are statistical and systematic, respectively. This Belle result is consistent with the previous measurement from the CLEO experiment but has a fivefold improvement in precision. By combining our result with the world average $\mathcal{B}(\Lambda_c^+ \rightarrow pK^-\pi^+)$, we obtain the absolute branching fraction $\mathcal{B}(\Lambda_c^+ \rightarrow pK_S^0\pi^0) = (2.12 \pm 0.01 \pm 0.05 \pm 0.10)\%$, where the uncertainties are statistical, systematic, and the uncertainty in the absolute branching fraction scale $\mathcal{B}(\Lambda_c^+ \rightarrow pK^-\pi^+)$, respectively. This measurement can shed light on hadronic decay mechanisms in charmed baryon decays.

I. INTRODUCTION

The nonleptonic weak decays of Λ_c^+ provide a unique testing ground for understanding the factorization scheme involving the $c \rightarrow s$ transition and the final-state interactions. Among the possible final states, $N\bar{K}\pi$ decays are particularly useful for examining the

isospin properties of the weak interaction in Λ_c^+ decay [1]. The $\Delta S = 1$ Cabibbo-allowed transition is governed by $c \rightarrow s\bar{u}d$, so iso-singlet Λ_c^+ decays result in a final state with $I = I_3 = 1$. In the $\Lambda_c^+ \rightarrow N\bar{K}\pi$ decays, the $N\bar{K}$ state can have isospin 0 or 1. Thus, the sum of isospin amplitudes of the three decay modes, $\sqrt{2}\mathcal{A}(p\bar{K}^0\pi^0) + \mathcal{A}(pK^-\pi^+) + \mathcal{A}(n\bar{K}^0\pi^+)$, is zero according to isospin symmetry [2–4], which imposes useful constraints on the branching ratios of the nonleptonic decay channels. In the quark-diagram schemes for $\Lambda_c^+ \rightarrow N\bar{K}\pi$ decays, as shown in Fig. 1, direct π^+ emission can involve a color-allowed factorizable process with external W^+ emission (Fig. 1(c)) but a π^0 cannot be produced in this process. The dominant contributions in the $N\bar{K}\pi^0$ decays instead are from color-suppressed internal W^+ emission and internal flavor conversion involving the subprocess $cd \rightarrow su$ with W^+ exchange.

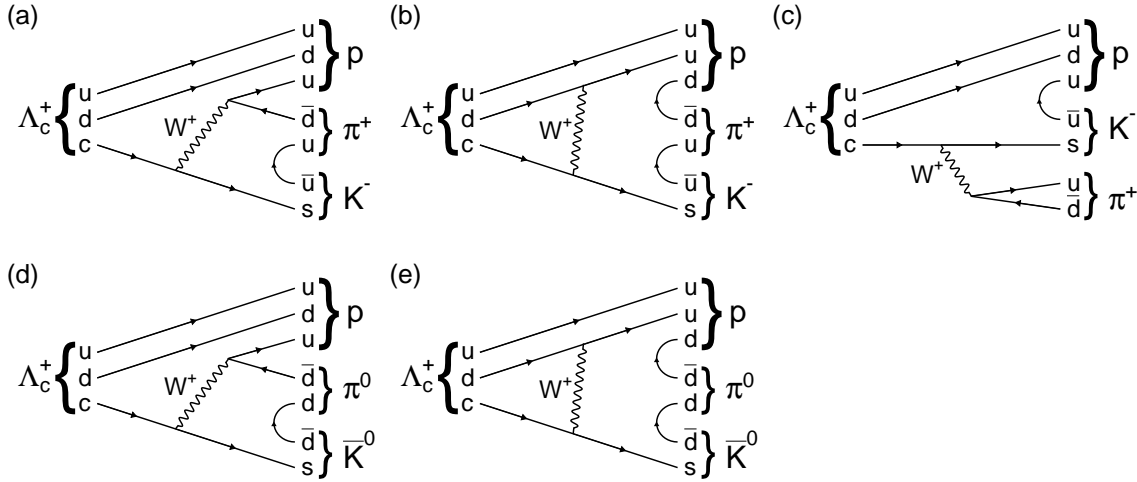


FIG. 1. Typical Feynman diagrams for internal W emission (a), internal W exchange (b), and external W emission (c) processes in $\Lambda_c^+ \rightarrow pK^-\pi^+$ decays, and internal W emission (d) and internal W exchange (e) processes in $\Lambda_c^+ \rightarrow pK_S^0\pi^0$ decays.

Since direct π^+ emission leaves the ud diquark in the iso-singlet Λ_c^+ as a spectator, the sud cluster in the final state is a pure $I = 0$ state, thus favoring the $I = 0$ $\bar{K}N$ state [5, 6]. Hence, if the direct π^+ emission process is dominant, the two-body decay $\Lambda_c^+ \rightarrow \Lambda\pi^+$ should be greatly favored over $\Lambda_c^+ \rightarrow \Sigma^0\pi^+$. Moreover, as the Λ_c^+ contains an anti-symmetric quark pair $(ud - du)c$, factorizable processes are suppressed for Λ_c^+ decays involving a baryon decuplet with totally flavor symmetric quark content [7]. However, the experimentally determined branching fractions for the two decays are comparable, indicating that the contributions from color-suppressed W^+ emission and W^+ exchange processes are large. The rescattering

of the $N\pi$ pair in the final state can populate $N(1535)$ and $N(1650)$ resonances, and the $N\bar{K}$ final-state interaction generates $\Lambda(1405)$ and $\Lambda(1670)$ states [8].

An observation of a narrow structure at the $\Lambda\eta$ threshold in the K^-p invariant mass spectrum in $\Lambda_c^+ \rightarrow pK^-\pi^+$ reported by the Belle collaboration [9] has attracted significant attention. A recent analysis, attempting to shed light on the nature of the structure, indicates a $\Lambda\eta$ cusp effect, enhanced by the $\Lambda(1670)$ pole [10]. Another study suggests that the effect giving rise to the narrow structure is enhanced by a triangle singularity involving rescattering via the near-lying $\Lambda a_0(980)^+$ or $\eta\Sigma(1660)^+$ scattering [11]. In $\Lambda_c^+ \rightarrow pK^-\pi^+$ process, isospin symmetry implies that the partial branching ratio of $\Lambda_c^+ \rightarrow \Sigma^{*0}\pi^+$ equals that of $\Lambda_c^+ \rightarrow \Sigma^{*+}\pi^0$, whereas the $\Lambda_c^+ \rightarrow \Delta^{++}K^-$ decay is three times larger than the branching fraction of $\Lambda_c^+ \rightarrow \Delta^+\bar{K}^0$ [7, 12]. In the $\Lambda_c^+ \rightarrow p\bar{K}^0\pi^0$ decay, only Σ^{*+} resonances are possible in the $N\bar{K}$ system. Therefore, a precise measurement of the relative branching fraction for $\Lambda_c^+ \rightarrow pK_S^0\pi^0$ as well as the investigation of intermediate resonances provides stringent tests of isospin symmetry and could help to better understand non-factorizable processes in the non-leptonic decay of charmed baryons.

The absolute branching fractions for $\Lambda_c^+ \rightarrow n\bar{K}^0\pi^+$ and $\Lambda_c^+ \rightarrow pK_S^0\pi^0$ decays are reported from BESIII to be $\mathcal{B}(\Lambda_c^+ \rightarrow nK_S^0\pi^+) = (1.82 \pm 0.25)\%$ and $\mathcal{B}(\Lambda_c^+ \rightarrow pK_S^0\pi^0) = (1.87 \pm 0.14)\%$, respectively [3]. The branching fraction of $\Lambda_c^+ \rightarrow pK_S^0\pi^0$ relative to $\Lambda_c^+ \rightarrow pK^-\pi^+$ reported from CLEO is 0.33 ± 0.05 [13]. Here we report a precise measurement of the relative branching fraction of $\Lambda_c^+ \rightarrow pK_S^0\pi^0$ compared with $\Lambda_c^+ \rightarrow pK^-\pi^+$ using Belle data. In addition, we present the first investigation of the intermediate resonances in $\Lambda_c^+ \rightarrow pK_S^0\pi^0$ decays.

II. THE DATA SAMPLE AND THE BELLE DETECTOR

The branching fractions are measured based on a data sample obtained at or near $\Upsilon(1S)$, $\Upsilon(2S)$, $\Upsilon(3S)$, $\Upsilon(4S)$ and $\Upsilon(5S)$ with the Belle detector at the KEKB asymmetric energy e^+e^- collider [14]. The full Belle data sample has an integrated luminosity of 980 fb^{-1} . The Belle detector was a large-solid-angle magnetic spectrometer comprising a silicon vertex detector (SVD), a central drift chamber (CDC), an array of aerogel threshold Cherenkov counters (ACC), a barrel-like arrangement of time-of-flight scintillation counters (TOF), and an electromagnetic calorimeter comprising CsI(Tl) crystals (ECL) located inside a superconducting solenoid that provided a 1.5 T magnetic field. An iron flux return located

outside the coil was employed to detect K_L^0 mesons and identify muons. The Belle detector is described in detail in Ref. [15].

The Monte Carlo (MC) samples used in the simulation studies are generated using EvtGen [16] and PYTHIA [17], and propagated through a GEANT3 model of the full detector [18]. The final-state radiation process is simulated using the PHOTOS [19] package in EvtGen. A signal MC sample is generated via $e^+e^- \rightarrow c\bar{c} \rightarrow \Lambda_c^+ + X$ to study the reconstruction efficiency and signal shape functions. A Belle generic MC simulated data sample including $\Upsilon(4S) \rightarrow B\bar{B}$, $\Upsilon(5S) \rightarrow B_{(s)}^{(*)}\bar{B}_{(s)}^{(*)}$, $\Upsilon(1S, 2S, 3S)$ decays and $e^+e^- \rightarrow q\bar{q}$ ($q = u, d, s, c$) with the same integrated luminosity as the data is used to optimize the selection criteria.

III. EVENT SELECTION

We reconstruct $\Lambda_c^+ \rightarrow pK_S^0\pi^0$ with $K_S^0 \rightarrow \pi^+\pi^-$ and $\pi^0 \rightarrow \gamma\gamma$. The event selection criteria are optimized using a generic MC sample, with a figure-of-merit (FoM) defined as $N_{\text{sig}}/\sqrt{N_{\text{sig}} + N_{\text{bkg}}}$, where N_{sig} is the number of signal events and N_{bkg} is the number of background events. The latter are obtained in the $pK_S^0\pi^0$ invariant mass region between 2.263 GeV/ c^2 and 2.306 GeV/ c^2 .

The likelihood \mathcal{L}_i ($i = \pi^\pm, K^\pm, p^\pm$) is calculated by combining information from the ACC, CDC, and TOF detectors. The likelihood ratio between hypotheses i and i' is defined as $\mathcal{R}(i|i') = \mathcal{L}_i/(\mathcal{L}_i + \mathcal{L}_{i'})$. Charged tracks must satisfy $\mathcal{R}(p|K) > 0.9$ and $\mathcal{R}(p|\pi) > 0.9$ to be considered as proton candidates. Furthermore, the electron likelihood ratio ($\mathcal{R}(e)$), obtained from ACC, CDC, and ECL information, should be smaller than 0.9 for the proton candidates. For all proton candidates, the distance-of-closest-approach (DOCA) to the beam interaction point (IP) must be smaller than 2.0 cm along the beam direction (z) and smaller than 0.1 cm in the transverse direction (r). Furthermore, at least one hit in SVD is required. After applying the selection criteria, the PID efficiency for proton candidates is 83% in the typical momentum range of Λ_c^+ decays.

We reconstruct K_S^0 candidates using pairs of oppositely charged particles assumed to be pions. We use a neural network algorithm involving the K_S^0 momentum in the laboratory frame, the distance between two charged pion tracks along the z axis, the flight length of K_S^0 projected onto the r plane, the angle between the K_S^0 momentum and the vector from IP to K_S^0 decay vertex in the laboratory frame, longer and shorter DOCAs in the r -direction

of charged pions, the angle between the K_S^0 momentum in the laboratory frame and the charged pion momentum in the K_S^0 rest frame, the number of CDC hits from each π^\pm track and the presence or absence of SVD hits [20]. In addition, we perform a mass-constrained fit to the K_S^0 candidates in order to improve the K_S^0 momentum resolution. The χ^2 value of the mass-constrained vertex fit to the π^+ and π^- tracks with a common vertex is required to be smaller than 40.

ECL clusters that do not have matching tracks in the CDC are identified as photons, and the π^0 candidates are reconstructed from photon pairs. For each photon, the energy deposited in the ECL must exceed 50 (100) MeV if the cluster is found in the barrel (end-cap) region [15]. The ratio of energy deposits in the 3×3 array of crystals, centered in the crystal with the highest energy, to that of 5×5 crystal array must exceed 0.9. We select the π^0 candidates within the $M(\gamma\gamma)$ range from 120 MeV/ c^2 to 150 MeV/ c^2 , corresponding to approximately three standard deviations (σ) in the $M(\gamma\gamma)$ resolution. The momentum of the π^0 candidate must be greater than 400 MeV/ c in the laboratory frame. A mass-constrained fit is also performed on the π^0 candidates to improve their momentum resolution.

As a final step, the proton, K_S^0 , and π^0 candidates are combined to reconstruct Λ_c^+ candidates. The scaled momentum x_p is defined as $x_p = p^*c/\sqrt{s/4 - M^2c^4}$, where p^* is the momentum of the Λ_c^+ candidate in the center-of-mass frame, s is the square of the beam center-of-mass energy and M is invariant mass of the Λ_c^+ candidate. The requirement $x_p > 0.54$ reduces the combinatorial background, particularly from B meson decays. We perform a vertex fit to the three decay products requiring the reconstructed K_S^0 and π^0 originate from the Λ_c^+ decay vertex. The χ^2 value of the vertex fit is required to be smaller than 40.

For $\Lambda_c^+ \rightarrow pK^-\pi^+$ decays, we reconstruct Λ_c^+ candidates using the event selection criteria typically used in other Λ_c^+ analyses with Belle [9], except that the x_p cut-off value is the same as in $\Lambda_c^+ \rightarrow pK_S^0\pi^0$ decays. For proton candidates, the same selection criteria are used as in our signal mode. For K^- and π^+ candidates, the requirements on $\mathcal{R}(e)$, DOCAs in z - and r -directions, and SVD hits are identical to those for proton candidates. However, the PID requirements are $\mathcal{R}(K|\pi) > 0.9$ and $\mathcal{R}(K|p) > 0.4$ for K^- and $\mathcal{R}(\pi|K) > 0.4$ and $\mathcal{R}(\pi|p) > 0.4$ for π^+ . The PID efficiencies of K and π are 82% and 94%, respectively, in the typical momentum range of the decays. We fit the three decay products to a common vertex. The χ^2 value of the vertex fit is required to be smaller than 40.

After applying all the selection criteria to the data, we observe an average of 1.04 and 1.02 candidates per event for the $\Lambda_c^+ \rightarrow pK_S^0\pi^0$ and $\Lambda_c^+ \rightarrow pK^-\pi^+$ modes within the invariant mass ranges $2.263 \text{ GeV}/c^2 < M(pK_S^0\pi^0) < 2.306 \text{ GeV}/c^2$ and $2.274 \text{ GeV}/c^2 < M(pK^-\pi^+) < 2.298 \text{ GeV}/c^2$, respectively. In addition, we find that approximately 4.0% and 1.8% of events in these modes contain multiple signal candidates. Since these multiple candidates do not contribute to the peaking background in a study of the generic MC simulation sample, we retain all candidates for further analysis.

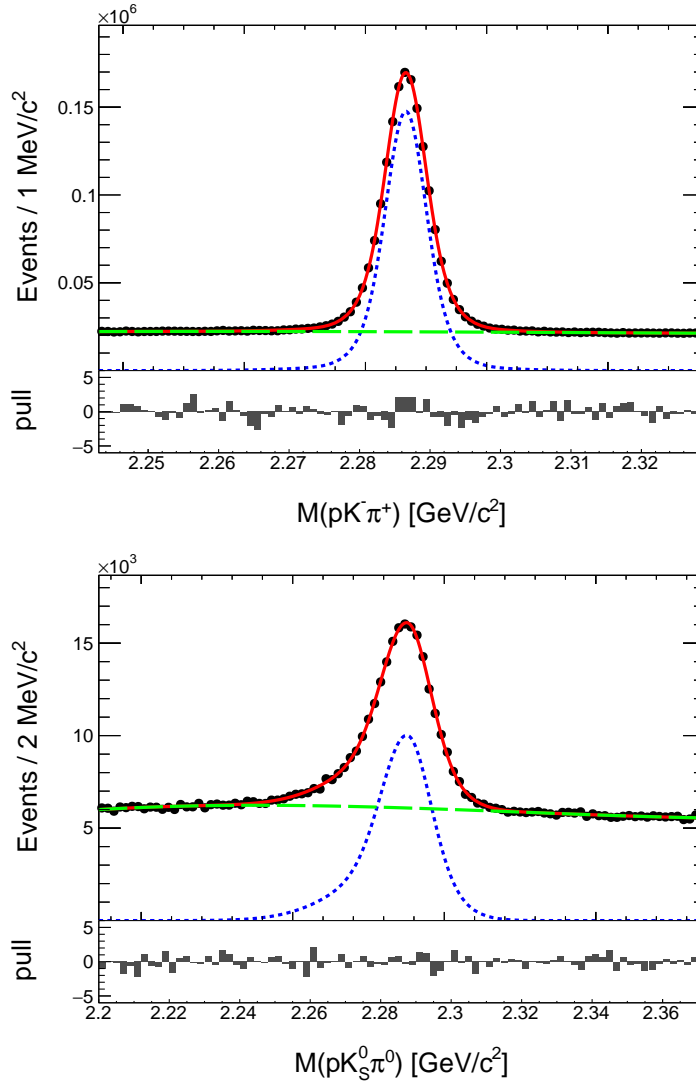


FIG. 2. Invariant mass distributions of Λ_c^+ candidates and fit results for $\Lambda_c^+ \rightarrow pK^-\pi^+$ (top) and $\Lambda_c^+ \rightarrow pK_S^0\pi^0$ (bottom). The total fit, signal, and background are shown by solid red, dashed blue, and long dashed green curves, respectively.

IV. SIGNAL EXTRACTION AND EFFICIENCY CORRECTION

Figure 2 shows the $M(pK^-\pi^+)$ and $M(pK_S^0\pi^0)$ distributions after applying the event selection method described in the previous section. We perform a binned extended maximum likelihood fit to extract the signal decay yields from the invariant mass distributions. The Λ_c^+ signal peak in the $M(pK^-\pi^+)$ distribution, which corresponds to mass resolution due to detector response, is parameterized by a sum of two Gaussian functions and one bifurcated Gaussian function, with each function sharing a common mean. To accurately model the energy loss associated with π^0 daughter γ 's in the $\Lambda_c^+ \rightarrow pK_S^0\pi^0$ decay, its signal function is taken as the sum of two bifurcated Gaussian functions sharing a common mean. A third-order polynomial function represents the combinatorial backgrounds for $M(pK^-\pi^+)$ and $M(pK_S^0\pi^0)$ fits. The extracted Λ_c^+ yields for $\Lambda_c^+ \rightarrow pK^-\pi^+$ and $\Lambda_c^+ \rightarrow pK_S^0\pi^0$ decays are $(1.405 \pm 0.003) \times 10^6$ and $(1.283 \pm 0.010) \times 10^5$, respectively, where the uncertainties are purely statistical.

The mass resolution parameters obtained by the fit for $\Lambda_c^+ \rightarrow pK^-\pi^+$ decay are as follows: two Gaussians with σ values of (3.17 ± 0.02) MeV/ c^2 and (4.80 ± 0.07) MeV/ c^2 respectively, and a bifurcated Gaussian with $\sigma_{\text{left}} = (19.5 \pm 0.39)$ MeV/ c^2 and $\sigma_{\text{right}} = (10.9 \pm 0.32)$ MeV/ c^2 . The yield fractions for the two Gaussians are $(50.2 \pm 1.3)\%$ and $(42.3 \pm 0.6)\%$. For $\Lambda_c^+ \rightarrow pK_S^0\pi^0$ decay, there are two bifurcated Gaussians with σ_{left} and σ_{right} as follows: (8.19 ± 0.23) MeV/ c^2 and (7.31 ± 0.27) MeV/ c^2 for the first Gaussian, and (19.5 ± 0.22) MeV/ c^2 and (11.6 ± 0.30) MeV/ c^2 for the second Gaussian. The yield ratio of the first Gaussian to the second is 1.07 ± 0.07 . The uncertainties of these values are statistical only.

As the reconstruction efficiency varies across the phase space of the Dalitz plot, as shown in Fig. 3, we apply a bin-by-bin correction to estimate the efficiency-corrected yields of both decays. To improve the resolution of the Dalitz plots, we fit the trajectories of the Λ_c^+ daughters to a common vertex and use a Λ_c^+ mass constraint. The efficiency-corrected yield y^{corr} calculated via $y^{\text{corr}} = \sum_i \frac{y_i}{\epsilon_i}$, where y_i and ϵ_i are the extracted yield and reconstruction efficiency of i -th bin in the Dalitz plots, respectively. In this correction, the Dalitz plots are divided into 5×10 bins for both decays, as shown in Fig. 4. Note that the bin width of the Dalitz plots is much larger than the resolution of the data, so the effect of bin migration on y_i is negligible.

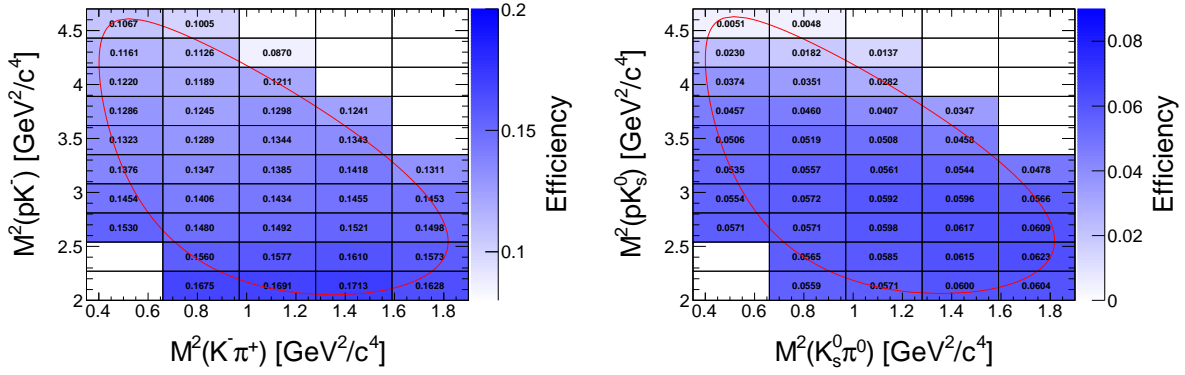


FIG. 3. Distributions of average reconstruction efficiencies over the Dalitz plots divided into the 10×5 bins of $M^2(pK)$ vs. $M^2(K\pi)$ for the $\Lambda_c^+ \rightarrow pK^-\pi^+$ (left) and the $\Lambda_c^+ \rightarrow pK_S^0\pi^0$ (right). Red contours represent the kinematic boundaries of the Dalitz plot, assuming the nominal Λ_c^+ mass.

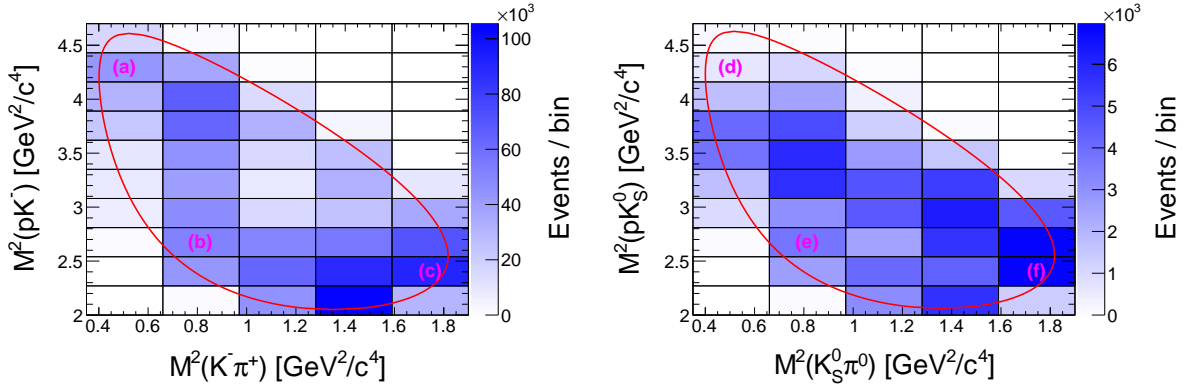


FIG. 4. Extracted signal yield for each Dalitz bin for $\Lambda_c^+ \rightarrow pK^-\pi^+$ (left) and $\Lambda_c^+ \rightarrow pK_S^0\pi^0$ (right). Fit results in the sample bins labeled from (a) to (f) are shown in Fig. 5. Red contours represent the Dalitz plot boundaries assuming the nominal Λ_c^+ mass.

The yield for each bin is determined using the same functions employed for the overall event fit. However, all lineshape parameters, except for a common scaling factor applied to all Gaussian widths, are fixed at the values obtained from corresponding signal MC samples. This scaling factor corrects for the resolution difference between the data and the MC simulation. The fitting results for typical bins are shown in Fig. 5. We determine the efficiency-corrected yields as $(9.570 \pm 0.012) \times 10^6$ for $\Lambda_c^+ \rightarrow pK^-\pi^+$ and $(2.221 \pm 0.015) \times 10^6$ for $\Lambda_c^+ \rightarrow pK_S^0\pi^0$, where the uncertainties are statistical only. The bin-by-bin

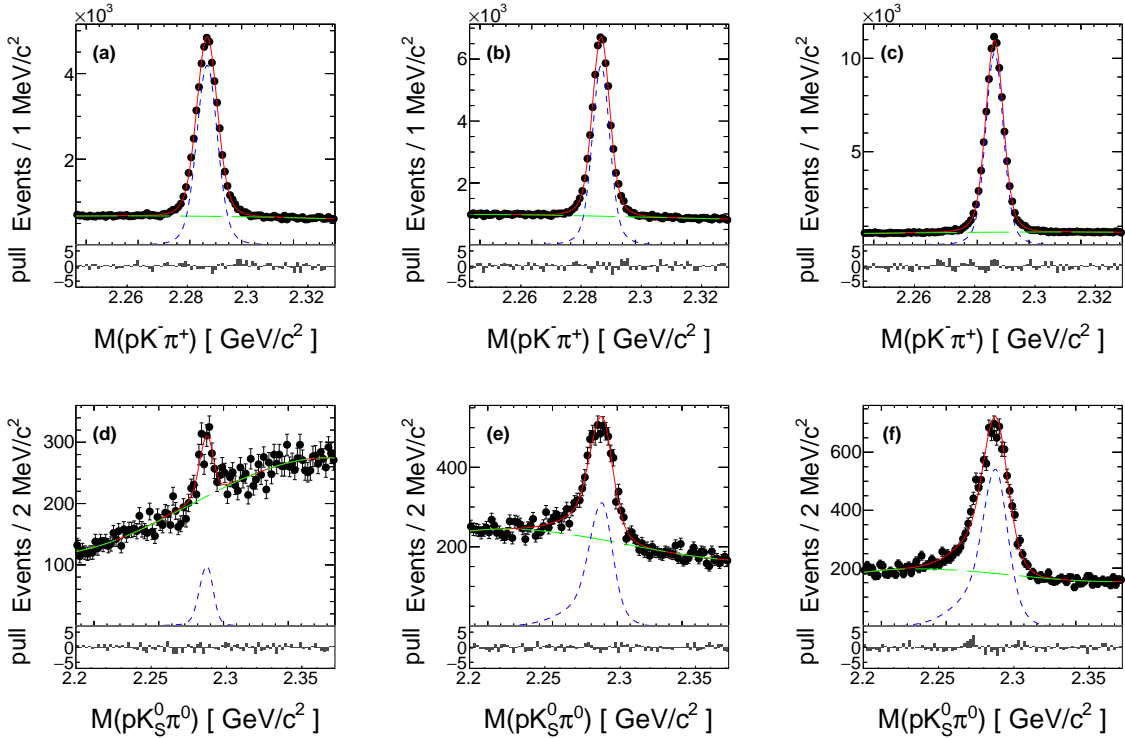


FIG. 5. Fit results (red curves) in the sample Dalitz plot bins specified in Fig. 4 for (a-c) $\Lambda_c^+ \rightarrow pK^-\pi^+$ and (d-f) $\Lambda_c^+ \rightarrow pK_S^0\pi^0$ decays. The dashed blue and long dashed green curves represent the signal and background, respectively.

correction method enables the extraction of efficiency-corrected yields, without requiring specific models for the production of intermediate states.

V. BRANCHING FRACTION

The relative branching fraction is calculated using the following equation,

$$\frac{\mathcal{B}(\Lambda_c^+ \rightarrow pK_S^0\pi^0)}{\mathcal{B}(\Lambda_c^+ \rightarrow pK^-\pi^+)} = \frac{y^{corr}(\Lambda_c^+ \rightarrow pK_S^0\pi^0)}{y^{corr}(\Lambda_c^+ \rightarrow pK^-\pi^+) \times \mathcal{B}(\pi^0 \rightarrow \gamma\gamma) \times \mathcal{B}(K_S^0 \rightarrow \pi^+\pi^-)}, \quad (1)$$

where we use $\mathcal{B}(\pi^0 \rightarrow \gamma\gamma) = (98.823 \pm 0.034)\%$ and $\mathcal{B}(K_S^0 \rightarrow \pi^+\pi^-) = (69.20 \pm 0.05)\%$ from Ref. [21]. By using Eq. (1) and the efficiency-corrected yields, the relative branching fraction is determined as follows:

$$\frac{\mathcal{B}(\Lambda_c^+ \rightarrow pK_S^0\pi^0)}{\mathcal{B}(\Lambda_c^+ \rightarrow pK^-\pi^+)} = 0.339 \pm 0.002, \quad (2)$$

where the uncertainty is statistical only.

By assuming that the sum of the amplitudes, $\sqrt{2}\mathcal{A}(p\bar{K}^0\pi^0) + \mathcal{A}(pK^-\pi^+) + \mathcal{A}(n\bar{K}^0\pi^+)$, is zero as described above, we can express the amplitudes in terms of two components, \mathcal{A}_0 and \mathcal{A}_1 , corresponding to the isospin amplitudes of the $I = 0$ and $I = 1$ states of the $N\bar{K}$ system, respectively [2, 3]. Defining a relative phase difference (δ), between \mathcal{A}_0 and \mathcal{A}_1 as $\mathcal{A}_1/\mathcal{A}_0 = |\mathcal{A}_1/\mathcal{A}_0|e^{i\delta}$, the relationship between the branching fractions and the isospin amplitudes is given by the following equations,

$$\mathcal{B}(\Lambda_c^+ \rightarrow p\bar{K}^0\pi^0) = \frac{1}{2}|\mathcal{A}_1|^2, \quad (3)$$

$$\mathcal{B}(\Lambda_c^+ \rightarrow pK^-\pi^+) = \frac{1}{2}|\mathcal{A}_0|^2 + \frac{1}{4}|\mathcal{A}_1|^2 - \frac{1}{\sqrt{2}}|\mathcal{A}_0||\mathcal{A}_1|\cos\delta, \quad (4)$$

and

$$\mathcal{B}(\Lambda_c^+ \rightarrow n\bar{K}^0\pi^+) = \frac{1}{2}|\mathcal{A}_0|^2 + \frac{1}{4}|\mathcal{A}_1|^2 + \frac{1}{\sqrt{2}}|\mathcal{A}_0||\mathcal{A}_1|\cos\delta. \quad (5)$$

With the measured value of $\mathcal{B}(\Lambda_c^+ \rightarrow pK_S^0\pi^0)/\mathcal{B}(\Lambda_c^+ \rightarrow pK^-\pi^+)$ and the world average $\mathcal{B}(\Lambda_c^+ \rightarrow n\bar{K}^0\pi^+)/\mathcal{B}(\Lambda_c^+ \rightarrow pK^-\pi^+) = 0.581 \pm 0.084$ [21], $|\delta|$ was determined to be 1.842 ± 0.069 , while the relative strength ($|\mathcal{A}_1|/|\mathcal{A}_0|$) was found to be 1.23 ± 0.06 , where the uncertainty is the sum in quadrature of the statistical uncertainty and the uncertainty in $\mathcal{B}(\Lambda_c^+ \rightarrow n\bar{K}^0\pi^+)/\mathcal{B}(\Lambda_c^+ \rightarrow pK^-\pi^+)$. The results show that the isospin amplitude \mathcal{A}_1 is not significantly suppressed compared to \mathcal{A}_0 in Λ_c^+ decays. Here, we note that the calculation assumes isospin symmetry for the non-resonant contributions [2].

Figure 6 shows the Dalitz plot, $M^2(K_S^0\pi^0)$ vs. $M^2(pK_S^0)$ for $\Lambda_c^+ \rightarrow pK_S^0\pi^0$ decays, and several bands corresponding to intermediate resonances are observed in the plot. We investigate the intermediate resonances by projecting the Dalitz plot onto the one-dimensional distributions of $M(pK_S^0)$, $M(K_S^0\pi^0)$, and $M(p\pi^0)$. We apply efficiency corrections and then subtract non- Λ_c^+ background fitting the reconstructed Λ_c^+ mass distribution in each bin of plots with a similar method described in Section IV.

In the $M(pK_S^0)$ distribution and the Dalitz plot of the $\Lambda_c^+ \rightarrow pK_S^0\pi^0$, as shown in Fig. 7(a) and the left of Fig. 6, respectively, Σ^* hyperons are not as prominent. However, there are distinct peak structures that might be tentatively ascribed to $\Lambda(1520)$ and $\Lambda(1670)$ hyperons in the $M(pK^-)$ distribution, as shown in Fig. 7(b). This finding is in agreement with the expectation that Λ^* hyperons are preferred over Σ^* hyperons in the π^+ emission decays [5]. This could be attributed to their production dynamics being governed by color-suppressed factorizable process in the $\Lambda_c^+ \rightarrow pK_S^0\pi^0$ decay.

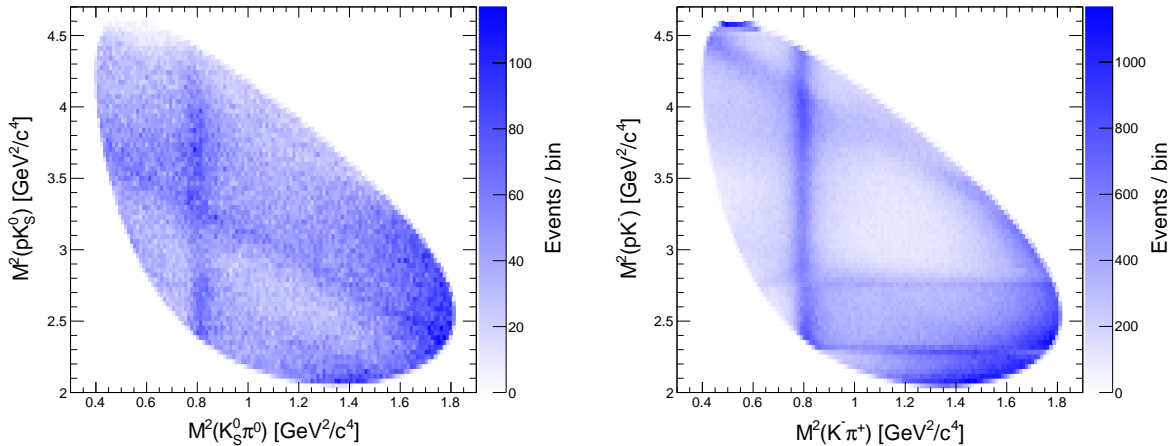


FIG. 6. Dalitz plots of the $\Lambda_c^+ \rightarrow pK_S^0\pi^0$ (left) and $\Lambda_c^+ \rightarrow pK^-\pi^+$ (right) channels within the regions $2.263 \text{ GeV}/c^2 < M(pK_S^0\pi^0) < 2.306 \text{ GeV}/c^2$ and $2.274 \text{ GeV}/c^2 < M(pK^-\pi^+) < 2.298 \text{ GeV}/c^2$, respectively. Both bin widths of x and y axes are $0.02 \text{ GeV}^2/c^4$. Non- Λ_c^+ background events shown in Fig. 2 are included in the Dalitz plots.

The peaking structure corresponding to $\Delta(1232)$ is much smaller in the $M(p\pi^0)$ distribution of the $\Lambda_c^+ \rightarrow pK_S^0\pi^0$ sample (Fig. 7(c)) compared to the one in the $M(p\pi^+)$ distribution for $\Lambda_c^+ \rightarrow pK^-\pi^+$ decays (Fig. 7(d)). This suppression can be attributed to the preference for the production of the $\Delta^{++}K^-$ channel over the $\Delta^+\bar{K}^0$ channel, as required by isospin symmetry. Furthermore, a clear peaking structure near the $p\eta$ mass threshold is evident in the $M(p\pi^0)$ distribution of $\Lambda_c^+ \rightarrow pK_S^0\pi^0$ decay. This peak corresponds to the diagonal band observed in the Dalitz plot to the left of Fig. 6. The same effect was observed in the $\Lambda_c^+ \rightarrow pK_S^0\eta$ study in Ref. [22]. The similarity of this effect and the $\Lambda\eta$ threshold cusp, which was found to be amplified by the $\Lambda(1670)$ in the pK^- system as shown in Fig. 7(b) [10, 23], suggests that the peak near the $p\eta$ threshold in the Fig. 7(c) may also be attributed to a threshold cusp enhanced by the $N(1535)^+$.

Both $\Lambda_c^+ \rightarrow pK^-\pi^+$ and $\Lambda_c^+ \rightarrow pK_S^0\pi^0$ decays exhibit a peaking structure corresponding to the vector resonance $K^*(892)^0$, as shown in Fig. 7(e) and (f). In the region where high-mass K^* mesons are expected, a clear enhancement with respect to phase space is seen in both decay modes. To further understand the role of isospin symmetry in the Λ_c^+ decays and extend our understanding of intermediate states such as Λ^* , Σ^* , Δ^* , and N^* resonances, an amplitude analysis with the helicity formalism of these two channels is planned for the

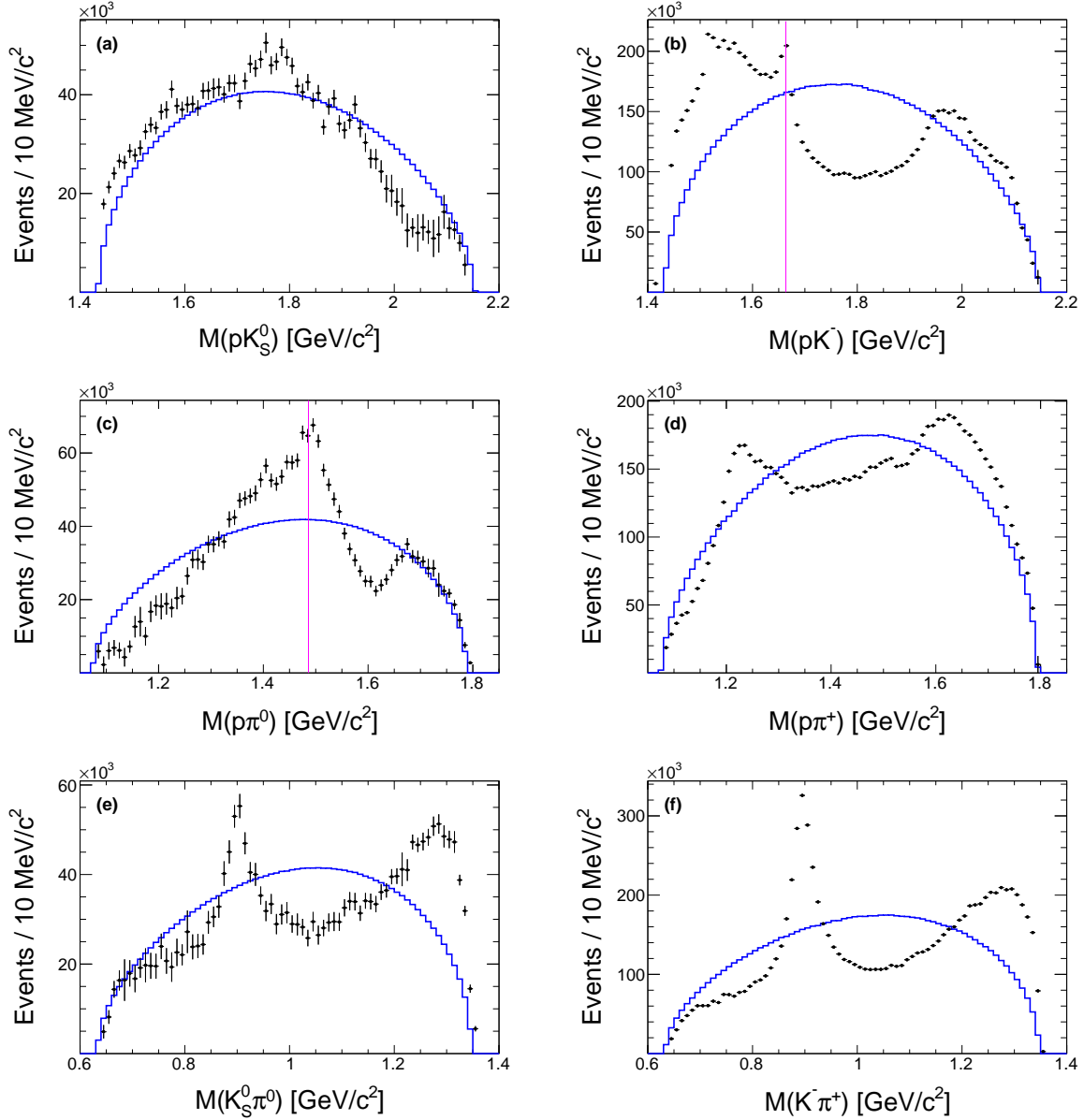


FIG. 7. Mass projection plots of $\Lambda_c^+ \rightarrow pK_S^0\pi^0$ (left) and $\Lambda_c^+ \rightarrow pK^-\pi^+$ (right) after background subtraction and efficiency correction. The projections of signal MC generated with a phase space model are superimposed in and shown as blue histograms. A strong enhancement near the $p\eta$ mass threshold is found in (c), and the $\Lambda\eta$ and $p\eta$ mass thresholds are marked in (b) and (c), respectively. A clear peaking structure at the K^* resonance is seen in the $K_S^0\pi^0$ system (e).

near future.

VI. SYSTEMATIC UNCERTAINTY

The systematic uncertainties of branching fractions are listed in Table I. The K_S^0 reconstruction imposes a systematic uncertainty that has been estimated using a control sample of $D^{*\pm} \rightarrow D^0\pi^\pm (D^0 \rightarrow K_S^0\pi^0)$ events. In the control sample study, the momentum-dependent K_S^0 reconstruction efficiency was compared between the data and MC samples. In a similar way, the π^0 reconstruction uncertainty was calibrated by a study in Ref. [24] using $\tau^- \rightarrow \pi^-\pi^0\nu_\tau$ events. Here, the difference in efficiency for $M(\gamma\gamma)$ selection between data and MC samples is also added in quadrature to the systematic uncertainty.

The uncertainty due to the background model shown in Fig. 5 is estimated by changing it to a second-order polynomial and a fourth-order polynomial. We estimate the systematic uncertainty resulting from the signal functions by performing one thousand fits, in which we vary the lineshape parameters fixed from the signal MC samples, within their respective statistical uncertainties. The systematic uncertainty is the standard deviation of the fit results. The quadratic sum of the systematic uncertainties arising from the background model and the signal function is referred to as “fit function” in Table I.

TABLE I. Sources of systematic uncertainties for the relative branching fraction, $\mathcal{B}(\Lambda_c^+ \rightarrow pK_S^0\pi^0)/\mathcal{B}(\Lambda_c^+ \rightarrow pK^-\pi^+)$.

Sources	Value (%)
K_S^0 reconstruction	1.57
π^0 reconstruction	1.54
Fit function	0.60
MC statistics	0.58
Dalitz plot binning	0.68
PID of K^- and π^+	0.34
Tracking of K^- and π^+	0.70
Total	2.57

We include the statistical uncertainty of the signal MC samples used in the efficiency

corrections across the Dalitz plots as a systematic uncertainty. We estimate the systematic uncertainties arising from the size of the Dalitz bins by modifying the Dalitz binning from the initial configuration of 5×10 to include the following configurations: 4×8 , 4×10 , 5×8 , 5×12 , 6×10 , and 6×12 . The largest difference obtained is attributed to a corresponding systematic uncertainty.

The systematic uncertainty from K^- and π^+ PIDs in $\Lambda_c^+ \rightarrow pK^-\pi^+$ decay is calculated based on the $D^{*+} \rightarrow D^0\pi^+(D^0 \rightarrow K^-\pi^+)$ control sample. Similar to the K_S^0 reconstruction, the PID efficiency as a function of momentum and polar angle in the laboratory frame is compared between data and MC samples. The systematic uncertainty attributed to tracking is 0.35% for each K^- and π^+ track in $\Lambda_c^+ \rightarrow pK^-\pi^+$ decay.

The uncertainties in the PDG values of $\mathcal{B}(\pi^0 \rightarrow \gamma\gamma)$ and $\mathcal{B}(K_S^0 \rightarrow \pi^+\pi^-)$ in Ref. [21] are negligible, so these contributions are not included in the systematic uncertainty. Other systematic uncertainties cancel out for the relative branching fraction measurements due to the similar kinematic distributions of the final state particles from $\Lambda_c^+ \rightarrow pK_S^0\pi^0$ and $\Lambda_c^+ \rightarrow pK^-\pi^+$ decays.

VII. SUMMARY

We study the $\Lambda_c^+ \rightarrow pK_S^0\pi^0$ decay using the full Belle dataset of 980 fb^{-1} at or near the $\Upsilon(nS)$ ($n = 1, 2, 3, 4$, and 5) resonances. The branching fraction of $\Lambda_c^+ \rightarrow pK_S^0\pi^0$ relative to $\Lambda_c^+ \rightarrow pK^-\pi^+$ is determined as

$$\frac{\mathcal{B}(\Lambda_c^+ \rightarrow pK_S^0\pi^0)}{\mathcal{B}(\Lambda_c^+ \rightarrow pK^-\pi^+)} = 0.339 \pm 0.002 \pm 0.009, \quad (6)$$

where the uncertainties are statistical and systematic, respectively. Using the PDG value of $\mathcal{B}(\Lambda_c^+ \rightarrow pK^-\pi^+) = (6.24 \pm 0.28)\%$ in Ref. [21], we obtain the following absolute branching fraction for $\Lambda_c^+ \rightarrow pK_S^0\pi^0$:

$$\mathcal{B}(\Lambda_c^+ \rightarrow pK_S^0\pi^0) = (2.12 \pm 0.01 \pm 0.05 \pm 0.10)\%, \quad (7)$$

where the uncertainties are statistical, systematic from this experiment and analysis, and due to the uncertainty in $\mathcal{B}(\Lambda_c^+ \rightarrow pK^-\pi^+)$, respectively. The measured branching fraction is consistent with the previous measurement by CLEO and has a fivefold improvement in precision [13].

Assuming isospin symmetry, we calculate that the ratio of the isospin amplitudes for $I = 1$ to $I = 0$ in the $N\bar{K}$ system is determined to be $1.23 \pm 0.03 \pm 0.06$, and the relative phase difference is obtained to be $1.842 \pm 0.001 \pm 0.069$, where the first uncertainty denotes the combined statistical and experimental systematic uncertainty and the second uncertainty is from the ratio $\mathcal{B}(\Lambda_c^+ \rightarrow n\bar{K}^0\pi^+)/\mathcal{B}(\Lambda_c^+ \rightarrow pK^-\pi^+)$. These values are consistent with previous results [3]. However, we do not find a strong enhancement due to Σ^* resonances in the $M(pK_S^0)$ distribution of $\Lambda_c^+ \rightarrow pK_S^0\pi^0$ decay. These results indicate that factors beyond isospin symmetry, such as resonant contributions, cannot be neglected.

In addition, we observe a clear peaking structure in the $p\pi^0$ system near the $p\eta$ threshold, which may be attributed to a threshold cusp enhanced by $N(1535)^+$. Further amplitude analysis is required to understand the contributions of intermediate resonances such as K^* , Λ^* , Σ^* , Δ^* , and N^* resonances, as well as to estimate the non-resonant contribution. Such a comprehensive approach will lead to stringent tests of isospin symmetry by comparing the partial branching ratios between $\Lambda_c^+ \rightarrow pK^-\pi^+$ and $\Lambda_c^+ \rightarrow pK_S^0\pi^0$ decays. This approach could also contribute to a better understanding of non-factorizable processes in the non-leptonic decay of charmed baryons.

ACKNOWLEDGMENTS

This work, based on data collected using the Belle II detector, which was built and commissioned prior to March 2019, and data collected using the Belle detector, which was operated until June 2010, was supported by Higher Education and Science Committee of the Republic of Armenia Grant No. 23LCG-1C011; Australian Research Council and Research Grants No. DP200101792, No. DP210101900, No. DP210102831, No. DE220100462, No. LE210100098, and No. LE230100085; Austrian Federal Ministry of Education, Science and Research, Austrian Science Fund (FWF) Grants DOI: 10.55776/P34529, DOI: 10.55776/J4731, DOI: 10.55776/J4625, DOI: 10.55776/M3153, and DOI: 10.55776/PAT1836324, and Horizon 2020 ERC Starting Grant No. 947006 “InterLeptons”; Natural Sciences and Engineering Research Council of Canada, Compute Canada and CANARIE; National Key R&D Program of China under Contract No. 2022YFA1601903, National Natural Science Foundation of China and Research Grants No. 11575017, No. 11761141009, No. 11705209, No. 11975076, No. 12135005, No. 12150004, No. 12161141008, No. 12475093, and No. 12175041, and

Shandong Provincial Natural Science Foundation Project ZR2022JQ02; the Czech Science Foundation Grant No. 22-18469S and Charles University Grant Agency project No. 246122; European Research Council, Seventh Framework PIEF-GA-2013-622527, Horizon 2020 ERC-Advanced Grants No. 267104 and No. 884719, Horizon 2020 ERC-Consolidator Grant No. 819127, Horizon 2020 Marie Skłodowska-Curie Grant Agreement No. 700525 “NIOBE” and No. 101026516, and Horizon 2020 Marie Skłodowska-Curie RISE project JENNIFER2 Grant Agreement No. 822070 (European grants); L’Institut National de Physique Nucléaire et de Physique des Particules (IN2P3) du CNRS and L’Agence Nationale de la Recherche (ANR) under Grant No. ANR-21-CE31-0009 (France); BMBF, DFG, HGF, MPG, and AvH Foundation (Germany); Department of Atomic Energy under Project Identification No. RTI 4002, Department of Science and Technology, and UPES SEED funding programs No. UPES/R&D-SEED-INFRA/17052023/01 and No. UPES/R&D-SOE/20062022/06 (India); Israel Science Foundation Grant No. 2476/17, U.S.-Israel Binational Science Foundation Grant No. 2016113, and Israel Ministry of Science Grant No. 3-16543; Istituto Nazionale di Fisica Nucleare and the Research Grants BELLE2, and the ICSC – Centro Nazionale di Ricerca in High Performance Computing, Big Data and Quantum Computing, funded by European Union – NextGenerationEU; Japan Society for the Promotion of Science, Grant-in-Aid for Scientific Research Grants No. 16H03968, No. 16H03993, No. 16H06492, No. 16K05323, No. 17H01133, No. 17H05405, No. 18K03621, No. 18H03710, No. 18H05226, No. 19H00682, No. 20H05850, No. 20H05858, No. 22H00144, No. 22K14056, No. 22K21347, No. 23H05433, No. 26220706, and No. 26400255, and the Ministry of Education, Culture, Sports, Science, and Technology (MEXT) of Japan; National Research Foundation (NRF) of Korea Grants No. 2016R1-D1A1B-02012900, No. 2018R1-A5A-1025563, No. 2018R1-A6A1A-06024970, No. 2020R1-A3B-2079993, No. 2021R1-A6A1A-03043957, No. 2021R1-C1C-2012925, No. 2021R1-F1A-1060423, No. 2021R1-F1A-1064008, No. 2022R1-A2C-1003993, No. 2022R1-A2C-1092335, No. RS-2023-00208693, No. RS-2024-00354342 and No. RS-2022-00197659, Radiation Science Research Institute, Foreign Large-Size Research Facility Application Supporting project, the Global Science Experimental Data Hub Center, the Korea Institute of Science and Technology Information (K24L2M1C4) and KREONET/GLORIAD; Universiti Malaya RU grant, Akademi Sains Malaysia, and Ministry of Education Malaysia; Frontiers of Science Program Contracts No. FOINS-296, No. CB-221329, No. CB-236394, No. CB-254409, and No. CB-180023, and SEP-CINVESTAV Re-

search Grant No. 237 (Mexico); the Polish Ministry of Science and Higher Education and the National Science Center; the Ministry of Science and Higher Education of the Russian Federation and the HSE University Basic Research Program, Moscow; University of Tabuk Research Grants No. S-0256-1438 and No. S-0280-1439 (Saudi Arabia), and Researchers Supporting Project number (RSPD2025R873), King Saud University, Riyadh, Saudi Arabia; Slovenian Research Agency and Research Grants No. J1-9124 and No. P1-0135; Ikerbasque, Basque Foundation for Science, the State Agency for Research of the Spanish Ministry of Science and Innovation through Grant No. PID2022-136510NB-C33, Agencia Estatal de Investigacion, Spain Grant No. RYC2020-029875-I and Generalitat Valenciana, Spain Grant No. CIDEAGENT/2018/020; the Swiss National Science Foundation; The Knut and Alice Wallenberg Foundation (Sweden), Contracts No. 2021.0174 and No. 2021.0299; National Science and Technology Council, and Ministry of Education (Taiwan); Thailand Center of Excellence in Physics; TUBITAK ULAKBIM (Turkey); National Research Foundation of Ukraine, Project No. 2020.02/0257, and Ministry of Education and Science of Ukraine; the U.S. National Science Foundation and Research Grants No. PHY-1913789 and No. PHY-2111604, and the U.S. Department of Energy and Research Awards No. DE-AC06-76RLO1830, No. DE-SC0007983, No. DE-SC0009824, No. DE-SC0009973, No. DE-SC0010007, No. DE-SC0010073, No. DE-SC0010118, No. DE-SC0010504, No. DE-SC0011784, No. DE-SC0012704, No. DE-SC0019230, No. DE-SC0021274, No. DE-SC0021616, No. DE-SC0022350, No. DE-SC0023470; and the Vietnam Academy of Science and Technology (VAST) under Grants No. NVCC.05.12/22-23 and No. DL0000.02/24-25.

These acknowledgements are not to be interpreted as an endorsement of any statement made by any of our institutes, funding agencies, governments, or their representatives.

We thank the SuperKEKB team for delivering high-luminosity collisions; the KEK cryogenics group for the efficient operation of the detector solenoid magnet and IBelle on site; the KEK Computer Research Center for on-site computing support; the NII for SINET6 network support; and the raw-data centers hosted by BNL, DESY, GridKa, IN2P3, INFN, PNNL/EMSL, and the University of Victoria.

[1] Unless otherwise noted, charge-conjugate modes are always implied throughout this paper.

[2] C. D. Lü, W. Wang and F. S. Yu, *Phys. Rev. D* **93**, 056008 (2016).

- [3] M. Ablikim *et al.* (BESIII Collaboration), Phys. Rev. Lett. **118**, 112001 (2017).
- [4] M. Gronau and J. L. Rosner, Phys. Rev. D **97**, 116015 (2018); M. Gronau, J. L. Rosner, and C. G. Wohl, Phys. Rev. D **98**, 073003 (2018).
- [5] K. Miyahara, T. Hyodo and E. Oset, Phys. Rev. C **92**, 055204 (2015).
- [6] J. K. Ahn *et al.*, Phys. Rev. D **100**, 034027 (2019).
- [7] Y. K. Hsiao, Q. Yi, S.-T. Cai, and H. J. Zhao, Eur. Phys. J. C **80**, 1067 (2020).
- [8] R. Pavao, S. Sakai, and E. Oset, Phys. Rev. C **98**, 015201 (2018); E. J. Garzon and E. Oset, Phys. Rev. C **91**, 025201 (2015).
- [9] S. B. Yang *et al.* (Belle Collaboration), Phys. Rev. Lett. **117**, 011801 (2016).
- [10] S. B. Yang *et al.* (Belle Collaboration), Phys. Rev. D. **108**, L031104 (2023).
- [11] X.-H. Liu, G. Li, J.-J. Xie, and Q. Zhao, Phys. Rev. D. **100**, 054006 (2019).
- [12] M. J. Savage and R. P. Springer, Phys. Rev. D **42**, 1527 (1990).
- [13] M. S. Alam *et al.* (CLEO Collaboration), Phys. Rev. D **57**, 4467-4470 (1998).
- [14] S. Kurokawa and E. Kikutani, Nucl. Instrum. Methods Phys. Res., Sect. A **499**, 1 (2003), and other papers included in this volume; T. Abe *et al.*, Prog. Theor. Exp. Phys. (**2013**), 03A001, and references therein.
- [15] A. Abashian *et al.* (Belle Collaboration), Nucl. Instrum. Methods Phys. Res., Sect. A **479**, 117 (2002); also see detector section in J. Brodzicka *et al.*, Prog. Theor. Exp. Phys. (**2012**), 04D001.
- [16] D. Lange, Nucl. Instrum. Methods Phys. Res., Sect. A **462**, 152 (2001).
- [17] T. Sjöstrand, S. Mrenna, and P. Skands, J. High Energy Phys. 05 (2006) 026.
- [18] R. Brun *et al.*, CERN Report No. DD/EE/84-1, 1984.
- [19] E. Barberio and Z. Was, Comput. Phys. Commun. **79**, 291 (1994).
- [20] H. Nakano *et al.* (Belle Collaboration), Phys. Rev. D **97**, 092003 (2018).
- [21] S. Navas *et al.* (Particle Data Group), Phys. Rev. D **110**, 030001 (2024).
- [22] L. K. Li *et al.* (Belle Collaboration), Phys. Rev. D **107**, 032004 (2023).
- [23] J. Y. Lee *et al.* (Belle Collaboration), Phys. Rev. D **103**, 052005 (2021).
- [24] S. Ryu *et al.* (Belle Collaboration), Phys. Rev. D **89**, 072009 (2014).